



Cite this: *Phys. Chem. Chem. Phys.*,
2019, **21**, 19054

Chemically-driven convective dissolution

M. Jotkar, * L. Rongy  and A. De Wit 

When a solute A dissolves in a host phase with a given solubility, the resulting density stratification is stable towards convection if the density profile increases monotonically along the gravity field. We theoretically and numerically study the convective destabilization by reaction of this dissolution when A reacts with a solute B present in the host phase to produce C via an $A + B \rightarrow C$ type of reaction. In this reactive case, composition changes can give rise to non-monotonic density profiles with a local maximum. A convective instability can then be triggered locally in the zone where the denser product overlies the less dense bulk solution. First, we perform a linear stability analysis to identify the critical conditions for this reaction-driven convective instability. Second, we perform nonlinear simulations and compare the critical values of the control parameters for the onset of convection in these simulations with those predicted by linear stability analysis. We further show that the asymptotic dissolution flux of A can be increased in the convective regime by increasing the difference $\Delta R_{CB} = R_C - R_B$ between the Rayleigh numbers of the product C and reactant B above a critical value and by increasing the ratio $\beta = B_0/A_0$ between the initial concentration B_0 of reactant B and the solubility A_0 of A . Our results indicate that chemical reactions can not only initiate convective mixing but can also give rise to large dissolution fluxes, which is advantageous for various geological applications.

Received 29th May 2019,
Accepted 13th August 2019

DOI: 10.1039/c9cp03044a

rsc.li/pccp

1 Introduction

Dissolution-driven convection has recently received significant attention owing to various geological applications such as CO_2 capture and sequestration (CCS) techniques for instance.¹ CCS involves capturing CO_2 at production sites and injecting it into geological storage sites such as saline aquifers. After injection under a cap rock, the less dense CO_2 accumulates on top of the denser brine. In this two-layer configuration, CO_2 can dissolve into the underlying brine. This results in denser CO_2 -rich brine lying on top of the less dense resident brine giving rise to an unstable density stratification, such that a buoyancy-driven fingering instability can develop. The convective motion facilitates increased mixing, which is desirable for improving the efficiency and safety of CO_2 sequestration process.^{2–8} The effect of chemical reactions on this nonlinear convective dissolution dynamics has been the subject of recent investigations.^{9–24} In particular, it has been shown that $A + B \rightarrow C$ reactions can accelerate or slow down dissolution-driven convection depending on the relative contribution to density of each of the species present in the host solution.^{11,12,16,19,21,22,24}

In some cases however, dissolution in the absence of reaction does not induce convection. This is the case either if the

dissolving species enters the host phase from above but decreases density or, on the contrary, if it enters the host solution from below but increases density. In these analogous situations, the density increases monotonically along the gravity field¹⁴ and diffusion remains the only transport process observed. It has been shown that chemical reactions are able to destabilize these situations and trigger convection by inducing a local extremum in the density profile.^{14,15,19,23,25}

Specifically, Loodts *et al.* conducted a linear stability analysis to show that positive growth rates and thus destabilization can be obtained when the reactive density profile features a local maximum.¹⁴ The variety of possible density profiles in the case where all species diffuse at different rates has been defined and connections to experimental results have been discussed.¹⁵ As an example, in a reaction involving the alkaline oxidation of glucose with methylene blue as a catalyst, it was demonstrated experimentally and theoretically that chemical reactions can induce convection in such an initially stable density stratification.^{26–29} Nonlinear simulations of the problem have also shown that, in this reaction-driven convective case, fingers develop not from the interface but from the maximum of density located below the interface.¹⁹ Similar conclusions have been obtained recently using a different boundary condition at the interface.²³ However, the critical values of the governing parameters for the onset of convection and the dissolution fluxes have not been characterized yet.

In this context, several important questions remain unanswered: in particular, how do the critical conditions for the onset of the

Université libre de Bruxelles (ULB), Faculté des Sciences, Nonlinear Physical Chemistry Unit, C.P. 231, 1050 Brussels, Belgium. E-mail: m.jotkar@ulb.ac.be, lrongy@ulb.ac.be, adewit@ulb.ac.be

convective instability obtained from nonlinear simulations compare against the predictions of linear stability theory? How do the asymptotic fluxes and the onset times for convection scale with the control parameters of the problem? Beyond the critical conditions, how does increasing the key parameters of the problem influence the convective dynamics?

To answer these questions, we study here theoretically such reaction-driven convective dissolution in partially miscible phases when the dissolving phase A lying above the host phase decreases the density of the host solution upon dissolution and reacts with a solute B to produce C via an $A + B \rightarrow C$ reaction. If all three species contribute to the density of the solution, it is possible to initiate buoyancy-driven convection depending on the relative properties of the reactant B and product C for a given A . We consider here equal diffusivities of the species to focus on the solutal effects. In particular, we study the effect on the asymptotic dissolution flux of A of varying the difference $\Delta R_{CB} = R_C - R_B$ in Rayleigh numbers of the product C and reactant B and of the ratio $\beta = B_0/A_0$ of the initial concentration B_0 of B with respect to the solubility A_0 of A . We first carry out a linear stability analysis using a frozen time or quasi-steady-state approximation to identify the critical conditions in the $(\beta, \Delta R_{CB})$ parameter space above which chemical reactions destabilize the density profiles and eventually lead to a convective instability. More precisely, we obtain the critical condition ΔR_{cr} as a function of β , above which the infinitesimal perturbations grow in time and destabilize the system. In a second part, we numerically study the nonlinear convective dynamics and compare the critical values of parameters for the onset of convection with those predicted by the linear stability analysis. We analyze the spatio-temporal dynamics using spacetime plots for the density and the temporal evolution of the dissolution flux in the parameter space. Finally, we show that the onset time for convection can be reduced by orders of magnitude and the asymptotic dissolution fluxes can be increased significantly upon increasing β and ΔR_{CB} above the critical value. Our results indicate that chemical reactions can not only induce convection but also enhance the storage rate substantially.

The article is organized as follows. In Section 2, we explain the numerical model used and classify the various convective regimes in Section 3. In Section 4, we present the methodology used for the linear stability analysis and the results obtained including the dispersion curves, the structure of the least stable eigenmode and the neutral stability boundary. Section 5 analyzes the nonlinear convective dynamics in the $(\beta, \Delta R_{CB})$ parameter space. Finally, we highlight the main findings of our work in Section 6.

2 Problem formulation

Following previous works,^{19,24} we consider a homogeneous, isotropic, isothermal porous medium in which two partially miscible aqueous phases are initially separated by a horizontal interface. The gravitational field \mathbf{g} points downwards along the vertical z axis and is perpendicular to the horizontal x axis.

The upper phase A dissolves into the lower host phase containing a reactant B with an initial concentration B_0 and reacts with B to produce C via a second order $A + B \rightarrow C$ reaction. All species contribute to the density of the solution and are assumed to diffuse at equal rates. We assume a local chemical equilibrium such that the concentration of A at the interface ($z = 0$) remains constant with time, and is equal to its finite solubility A_0 in the host phase. The concentrations of B and C are assumed to be small enough to not affect this solubility. The host phase extends from $x' = 0$ to $x' = L'$ in the horizontal direction and from $z' = 0$ to $z' = H'$ in the vertical direction. We focus on the density stratification problem which is stable in absence of reactions *i.e.* the case where the species A , dissolving from above, decreases the density of the host solution *i.e.* the Rayleigh number quantifying its contribution to density is negative. The problem is equivalent to the one where a species A increases the density of the host phase upon dissolution from below.¹⁴

The solute concentrations, time, spatial coordinates and velocity are non-dimensionalized using the following quantities:¹⁹

$$A = A'/A_0, \quad B = B'/A_0, \quad C = C'/A_0 \quad (1a)$$

$$t = t'/t_c, \quad z = z'/l_c, \quad \mathbf{u} = \mathbf{u}'/u_c, \quad (1b)$$

where the primes denote dimensional variables and we use the chemical time scale $t_c = 1/(qA_0)$ with q the kinetic constant of the reaction $A + B \rightarrow C$, the reaction–diffusion (RD) length scale $l_c = \sqrt{D_A t_c} = \sqrt{D_A/(qA_0)}$ with D_A the diffusion coefficient of A and the velocity scale $u_c = \phi l_c/t_c = \phi \sqrt{D_A q A_0}$ with ϕ the porosity of the medium.

The dimensionless reaction–diffusion–convection (RDC) equations governing the temporal evolution of the solute concentrations are

$$\frac{\partial A}{\partial t} + (\mathbf{u} \cdot \nabla)A = \nabla^2 A - AB, \quad (2a)$$

$$\frac{\partial C}{\partial t} + (\mathbf{u} \cdot \nabla)C = \nabla^2 C + AB, \quad (2b)$$

where \mathbf{u} is the two-dimensional velocity field. Since we assume that all the species diffuse at the same rate and that initially the host phase contains only B and no C , the dimensionless solute concentration of B can be reconstructed through the following conservation relation:

$$B = \beta - C, \quad (3)$$

where $\beta = B_0/A_0$.^{19,24} As convective dissolution is of importance in several applications in porous media, we consider here that the evolution of \mathbf{u} is given by Darcy's law:

$$\nabla p = -\mathbf{u} + \rho \mathbf{e}_z, \quad (4)$$

with p the dimensionless pressure and \mathbf{e}_z the unit vector along the gravity field.

Periodic boundary conditions are imposed at $x = 0$ and $x = L$, no vertical flow and no flux conditions are used for A and C at $z = H$ (bottom boundary) while at $z = 0$ (upper interface),

no vertical flow and no flux conditions for C are used along with $A = 1$. We solve the RDC eqn (2) with the initial conditions

$$A(x, z = 0, t = 0) = 1 + \varepsilon \cdot \text{rand}(x); \quad A(x, z > 0, t = 0) = 0, \quad (5a)$$

$$C(x, z, t = 0) = 0. \quad (5b)$$

Perturbations shown in eqn (5a) are introduced in the initial concentration of A at the interface in order to trigger the instability.^{30,31} $\varepsilon \ll 1$ is the amplitude of the perturbations, here chosen as 10^{-3} , and $\text{rand}(x)$ is their modulation along x , varying randomly between -1 and 1 ("white noise").

The equations are closed by an equation of state for the dimensionless density ρ , given as

$$\rho = R_A A + \Delta R_{CB} C, \quad (6)$$

where the Rayleigh numbers R_i ($i = A, B, C$) quantify the contribution to density of the species i as

$$R_i = \frac{\alpha_i A_0 g \kappa}{\phi \nu \sqrt{D_A q A_0}}, \quad (7)$$

where $\alpha_i = \frac{1}{\rho_0} \frac{\partial \rho'}{\partial c_i}$ is the solutal expansion coefficient of species i , ρ_0 is the dimensional density of the solvent, κ is the permeability and ν is the kinematic viscosity of the solvent. The difference in the contribution to density of C and B , defined as,

$$\Delta R_{CB} = R_C - R_B \quad (8)$$

and $\beta = B_0/A_0$ are the key parameters of the problem.

As shown previously,¹⁹ for equal diffusivities of the species considered here, the problem is completely determined by the three parameters: R_A , ΔR_{CB} and β . We recall that we focus here on the initially stable density stratification problem where the Rayleigh number of species A in eqn (7) is negative. We fix here arbitrarily $R_A = -1$ and study the effect of varying ΔR_{CB} and β .

We solve the RDC eqn (2) numerically along with eqn (4) and (6) and the relevant boundary conditions using the YALES³² software with the DARCY_SOLVER module. We use the computational domain width $L = 3072$ and height $H = 2048$ for most of the work such that the results are independent of the domain size. For particular destabilizing cases (mentioned later in Section 5), we have used a larger domain height $H = 4096$. The reader may refer to ref. 19 and 33 for further details on the numerics.

3 Classification of the density profiles

We recall that, when $R_A > 0$ and A dissolves from the top *i.e.* in the case where the non-reactive case is already buoyantly unstable, the various density profiles have already been classified in three main regimes: I (non-monotonic and stabilizing), II (monotonic and stabilizing) and III (monotonic and destabilizing).²⁴ We complement this classification for the $R_A < 0$ case here.

In the absence of chemical reactions, when $R_A < 0$ *i.e.* when the dissolving species A decreases the density of the host solution, the density profiles are monotonic and stable. In the reactive case with $R_A < 0$ and for equal diffusivities of the species, it is possible to obtain non-monotonic density profiles

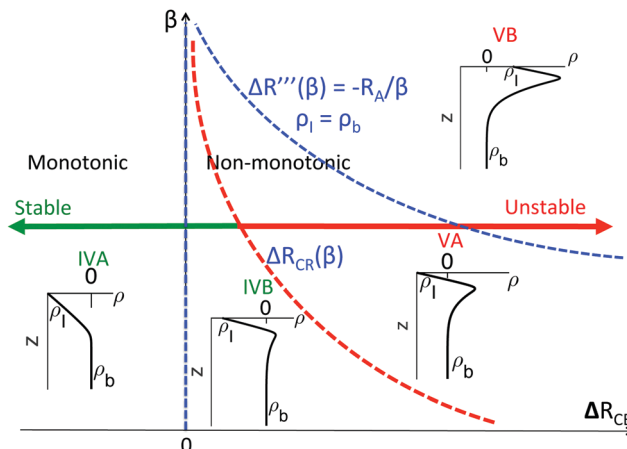


Fig. 1 Classification of the RD density profiles $\rho(z)$ in the $(\beta, \Delta R_{CB})$ space: regimes IVA (monotonic stable with $\rho_1 < \rho_b$), IVB (non-monotonic stable with $\rho_1 < \rho_b$), VA (non-monotonic unstable with $\rho_1 \leq \rho_b$) and VB (non-monotonic unstable with $\rho_1 > \rho_b$). The red dashed curve indicates the critical condition for instability, the vertical blue dashed line at $\Delta R_{CB} = 0$ indicates the transition from regime IVA to IVB and the blue dashed curve where $\Delta R''' = -R_A/\beta$ indicates the transition from regime VA to VB when $\rho_1 = \rho_b$. Here, ρ_1 is the density at the interface while ρ_b is the initial density of the host solution.

with a local maximum when $\Delta R_{CB} > 0$.¹⁴ The density ρ_1 at the interface ($z = 0$) where $A = 1$ and $C = \beta$ is equal to $\rho_1 = R_A + \beta \Delta R_{CB}$ while in the bulk, where $A = C = 0$, the initial density of the host solution is $\rho_b = 0$. In Fig. 1, the reaction-diffusion (RD) density profiles are classified into four regimes in the $(\beta, \Delta R_{CB})$ parameter space: regime IVA (monotonic, stable), regime IVB (non-monotonic, stable), regime VA (non-monotonic, unstable with $\rho_1 < \rho_b$) and regime VB (non-monotonic, unstable with $\rho_1 > \rho_b$).

When the product C is less dense than the reactant B ($\Delta R_{CB} < 0$), the density profiles in regime IVA are monotonic and buoyantly stable with the density at the interface smaller than the initial density of the host solution *i.e.* $\rho_1 < \rho_b$, similar to the non-reactive equivalent. When C is denser than B ($\Delta R_{CB} > 0$), the density profiles are non-monotonic with a local maximum. In regime IVB, the non-monotonic density profiles are stable and dominated by diffusion, similar to regime IVA. For a given β , above a certain critical value of ΔR_{CB} , referred to as ΔR_{cr} and determined by the linear stability analysis (explained in the following section and shown as the red dashed curve in Fig. 1), the non-monotonic density profiles are unstable.

These unstable density profiles can be further differentiated based on the amplitude of the end point values (ρ_1, ρ_b). The condition $\rho_1 = \rho_b$ gives trivially the curve $\Delta R''' = -R_A/\beta$ which separates regime VA where $\Delta R_{cr} \leq \Delta R_{CB} \leq \Delta R'''$ and $\rho_1 \leq \rho_b$ from regime VB where $\Delta R_{CB} > \Delta R'''$ and $\rho_1 > \rho_b$.

We now analyze the effect of varying positive ΔR_{CB} and β on the RD density profiles. For a given β , the local maximum of the density profile increases with increasing ΔR_{CB} as seen in Fig. 2(a). These profiles become unstable with respect to a buoyantly-driven instability beyond a critical ΔR_{CB} . As an example, the profiles with $\Delta R_{CB} = 0$ and 0.2 are in the stable regime IVB while those for $\Delta R_{CB} = 0.5$ and 1 belong to the unstable regime VA.

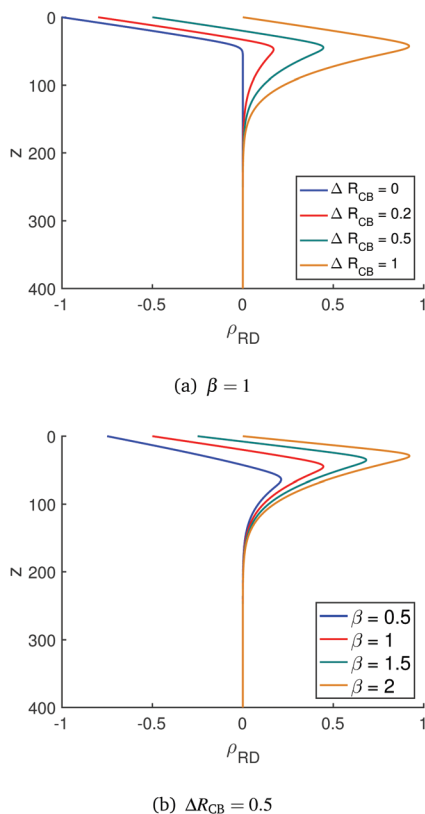


Fig. 2 Effect on the reaction–diffusion (RD) density profiles ρ_{RD} of varying (a) ΔR_{CB} at a fixed $\beta = 1$ and (b) β for a fixed $\Delta R_{CB} = 0.5$.

Similarly, the effect of increasing β for a given ΔR_{CB} is shown in Fig. 2(b), showing that the local maximum in the density profile increases with β . The density at the interface $\rho_I = R_A + \beta\Delta R_{CB}$ increases with β for a given ΔR_{CB} and R_A .

In this section, we have classified the density profiles for $R_A < 0$ into different regimes. In the subsequent sections, we identify the critical conditions for instability and study the nonlinear convective dynamics in regimes VA and VB, above the critical values of the parameters.

4 Linear stability analysis

To obtain the critical conditions for the convective instability *i.e.* the transition from the stable regime IVB to the unstable regime VA in the $(\beta, \Delta R_{CB})$ parametric space when $R_A = -1$, we carry out a linear stability analysis.

4.1 Methodology

Several methods have been used for studying the linear stability of time-dependent flows that involve different constraints or drawbacks linked to the initial assumptions and give different threshold times depending on how the perturbation growth is defined and measured.^{31,34,35} Recently, it has been shown that the onset time for convection measured experimentally during dissolution of CO_2 in pure water from above is well-captured by nonlinear simulations, whereas the onset times predicted by

linear stability analyses are an order of magnitude lower than the experimental findings.⁸ This indicates that the linear stability analysis is useful to give information on the relative stability of a given system when a parameter is varied but can not necessarily give the absolute value of the onset time. The technique of LSA is thus not crucial. We arbitrarily use here a frozen time approximation or quasi-steady-state-approximation (QSSA) and assume that the perturbations evolve much faster than the base state solutions such that these solutions can be considered to be frozen at a given time t_f . The base state profiles take the form $(\bar{A}, \bar{B}, \bar{C}, \bar{\psi} = 0)$ where Ψ is the streamfunction such that $u = -\partial\Psi/\partial z$ and $v = \partial\Psi/\partial x$. We then add the modal form of perturbations to these base state profiles as follows

$$(A, B, C, \Psi)(x, z, t) = (\bar{A}, \bar{B}, \bar{C}, 0)(z, t_f) + (\hat{a}, \hat{b}, \hat{c}, ik\hat{\psi})(z)e^{\sigma(t-t_f)+ikx} + \text{c.c.}, \quad (9)$$

with $i^2 = -1$, c.c. the complex conjugate, k the wavenumber and σ the growth rate of the perturbation. We substitute the modal form (9) in the reaction–diffusion–convection eqn (2)–(4)–(6) and neglect the nonlinear terms for the perturbation to derive the linearized governing equations.¹⁴ The derivatives in the z -direction are discretized using the Chebyshev–Gauss–Lobatto (CGL) collocation technique.³⁶ The resultant discretized problem is then solved as an eigenvalue problem

$$\underline{J} \cdot \underline{s} = \sigma \underline{s}, \quad (10)$$

where σ is the real eigenvalue and \underline{s} is the eigenvector. The eigenvalues are computed using the Arnoldi algorithm which reduces the original matrix \underline{J} in the eigenvalue formulation (10) to an upper Hessenberg matrix of a pre-specified dimension (m whose value is chosen to be 100) using the Krylov subspace iteration.³⁷ Typical values for the length of the numerical domain used is 500 and the number of CGL points used is 201, which are such that the assumption of semi-infinite domain holds true and the profiles are not affected by the lower boundary.

4.2 Dispersion curves

For $\beta = 1$, we find that $\Delta R_{cr} = 0.15$ is the critical value of ΔR_{CB} above which there exists at least one eigenmode with positive growth rate *i.e.* $\sigma > 0$ and the system is unstable. Dispersion curves representing the growth rate of the perturbation σ as a function of its wavenumber k for this critical value are shown in Fig. 3 at the different frozen times t_f indicated in the inset. The system is initially stable to buoyancy-driven convection since the growth rate σ is negative for all modes. After some initial transient, the buoyancy-driven instability is triggered when the local maximum in the density profile becomes sufficiently large. Subsequently, the growth rate σ changes sign and becomes positive for a given k . The maximum growth rate of the least stable mode occurs at $t_f = 2000$ and is of the order $\sigma_{\max} \sim 10^{-4}$ with a corresponding wavenumber $k_{\max} \approx 0.01$.

Typically, since the maximum growth rate for the critical value ΔR_{cr} is low ($\sim 10^{-4}$), the perturbation grows very slowly. At these conditions, the diffusive time scales are larger than the

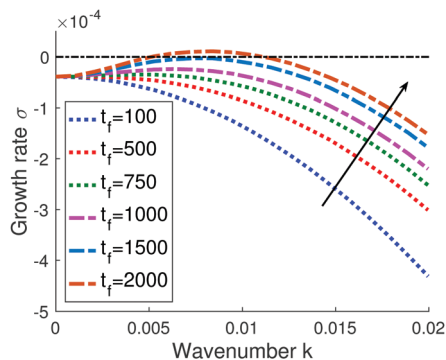


Fig. 3 Dispersion curves at different frozen times t_f indicated in the inset (arrow indicates the increasing values of t_f) for the critical value $\Delta R_{cr} = 0.15$ where $\sigma_{\max} = 0$ for $\beta = 1$, $R_A = -1$.

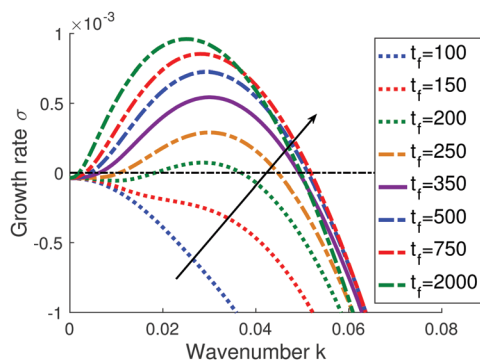
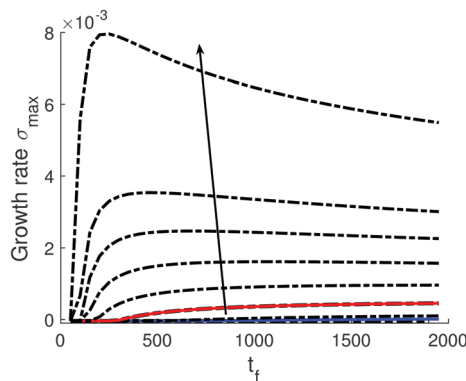


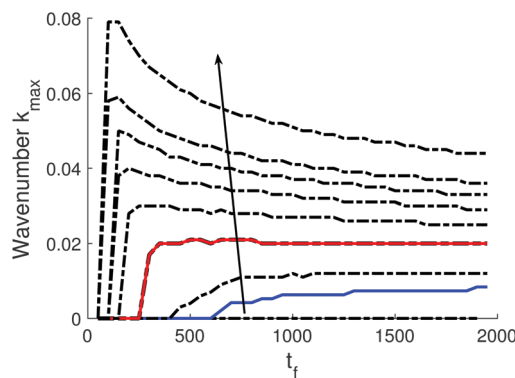
Fig. 4 Dispersion curves at different frozen times t_f indicated in the inset (arrow indicates the increasing values of t_f) for the critical value $\Delta R_{cr}' = 0.32$ where $\sigma_{\max} * t_f = 1$ for $\beta = 1$, $R_A = -1$.

time needed for this instability to become of order unity. Hence, the transport will continue to be diffusion-dominated. Therefore, following ref. 14 and 38, we also compute a characteristic growth rate σ_{\max}^* , defined as the maximum growth rate at t_f for which $\sigma_{\max} * t_f = 1$, such that the amplification factor $\exp(\sigma_{\max} * t_f)$ of the perturbation at t_f is large enough to trigger the convective instability. The corresponding characteristic wavenumber is referred to as k_{\max}^* . The critical value, referred to as $\Delta R_{cr}'$, is then the lowest value of ΔR_{CB} for a given β for which $\sigma_{\max} * t_f = 1$. For $\beta = 1$, the dispersion curves for this critical value $\Delta R_{cr}' = 0.32$ are shown in Fig. 4. The growth rates σ are of the order $\sim 10^{-3}$ and change sign from negative to positive at $t_f \approx 200$.

Using the dispersion curves at different frozen times, we extract in Fig. 5 the maximum growth rate σ_{\max} and the corresponding least stable wavenumber k_{\max} for increasing ΔR_{CB} indicated by the arrow for $\beta = 1$. Similar dispersion curves and plots for the maximum growth rate of the least stable eigenmode are obtained for different β as well (not shown here). Typically, σ_{\max} continues to grow with time up to a maximum value and then decreases (Fig. 5(a)). This asymptotic decrease occurs due to the weakening of the unstable density gradient by diffusion as time goes by. Subsequently, the wavenumber k_{\max} associated with the maximum growth rate also decreases monotonically as a function of time, as shown in Fig. 5(b).



(a)



(b)

Fig. 5 (a) Growth rate σ_{\max} and (b) wavenumber k_{\max} of the least stable mode as a function of the frozen time t_f for increasing $\Delta R_{CB} = 0.1, 0.15, 0.2, 0.3, 0.32, 0.4, 0.5, 0.6, 0.7, 1$ as indicated by the arrow with $\beta = 1$ and $R_A = -1$. The blue solid curves correspond to the neutrally stable condition $\Delta R_{cr} = 0.15$ in Fig. 3 where σ_{\max} changes sign from negative to positive. The red solid curves correspond to the critical condition $\Delta R_{cr}' = 0.32$, where $\sigma_{\max} * t_f = 1$.

4.3 Neutral boundary for instability

The results from the linear stability analysis are summarized in Fig. 6. The two different critical conditions ΔR_{cr} and $\Delta R_{cr}'$ are plotted in the $(\beta, \Delta R_{CB})$ parametric space. The neutral stability boundary ΔR_{cr} , where $\sigma_{\max} = 0$, separates the unstable regimes V from the stable regimes IV. For $\Delta R_{cr}'$ at which $\sigma_{\max} * t_f = 1$, the local maximum in the density profile is sufficiently large to trigger the convective instability in a relatively short time. We observe that both ΔR_{cr} and $\Delta R_{cr}'$ decrease with an increase in β , shrinking the stable regime VA below since an increase in either of these parameters leads to a larger local maximum in the density profiles (Fig. 2). We then compare these critical values for the convective instability obtained from linear stability analysis with nonlinear simulations. In the following section, we show that a good agreement is found for the critical conditions for the onset of convective instability between the simulations and the linear stability predictions given by $\Delta R_{cr}'$. We therefore refer to this value $\Delta R_{cr}'$ denoted by blue circles as the transition between regime IVB and VA in the rest of the article.

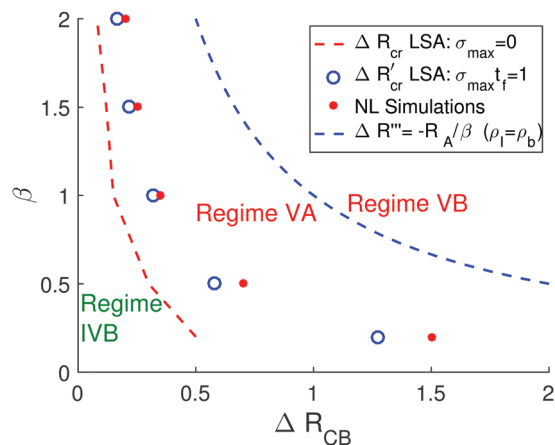


Fig. 6 Comparison of the stability boundaries in the $(\beta, \Delta R_{CB})$ parameter space given by the linear stability analysis (LSA) and the nonlinear (NL) simulations. The dashed red line corresponds to the neutral stability boundary ΔR_{cr} , where $\sigma_{\max} = 0$ separating the stable region below the curve and the unstable one above it. The solid blue circles indicate the critical values $\Delta R_{cr}'$ at which $\sigma_{\max} * t_f = 1$. The red dots indicate the critical values of ΔR_{CB} above which convection occurs in the nonlinear simulations. The dashed blue curve corresponds to the transition $\Delta R''' = -R_A/\beta$ from regime VA with $\rho_1 \leq \rho_b$ to regime VB with $\rho_1 > \rho_b$.

The dashed blue curve here represents $\Delta R'''$, the transition of the non-monotonic density profiles from regime VA ($\rho_1 \leq \rho_b$) to regime VB ($\rho_1 > \rho_b$). In all the cases studied here, we note that the transition $\Delta R'''$ from regime VA to VB occurs above the critical value for the convective instability. This indicates that the critical condition for the onset of the convection is solely determined by the formation of a sufficiently denser fluid layer locally overlying the less dense host phase below *i.e.* the occurrence of the non-monotonic density profiles with a local maximum of sufficiently large magnitude (regime VA).

To summarize this section, we have computed here the critical ΔR_{CB} as a function of β , referred to here as $\Delta R_{cr}'$, above which the convective instability occurs. In the next section, we study in detail the nonlinear convective dynamics and verify the predictions made by the linear stability analysis.

5 Nonlinear simulations

We now analyze the nonlinear convective dynamics in the reaction-driven unstable cases. We first study the effect of varying ΔR_{CB} for a particular β and then examine the effect of β in the subsequent subsection.

5.1 Convective dynamics for $\beta = 1$

For $\beta = 1$, the interface value ρ_1 of the non-monotonic density profile is equal to the initial value of the host solution ρ_b at $\Delta R''' = 1$. We find that in our nonlinear simulations, the critical value of ΔR_{CB} above which convection occurs is equal to 0.35. Below this value, the dominant transport mechanism is the diffusive one. This is in good agreement with the predictions made by linear stability analysis, where $\Delta R_{cr}' = 0.32$ for $\beta = 1$.

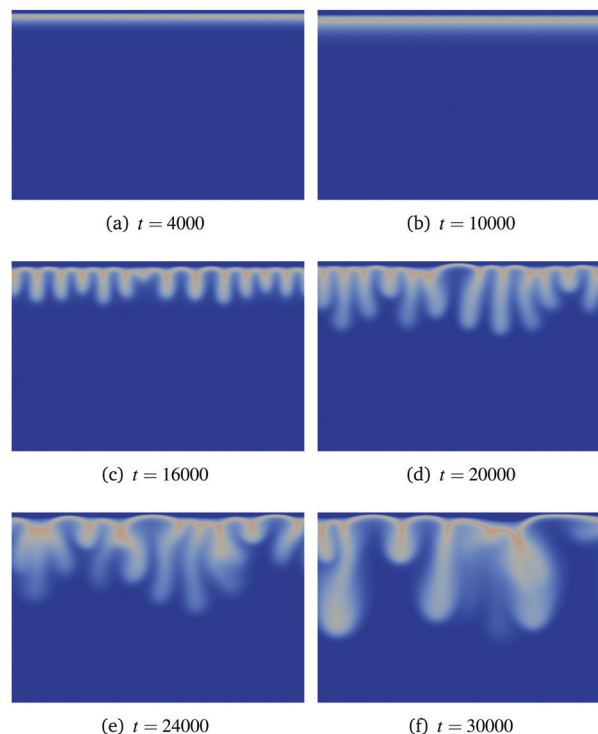


Fig. 7 Regime VA: density field at different times for $\beta = 1$, $\Delta R_{CB} = 0.5$ and $R_A = -1$. The scale varies between 0 (blue) and 0.73 (red).

We now look at the nonlinear dynamics in regime VA *i.e.* when $\Delta R_{cr}' < \Delta R_{CB} < \Delta R'''$. Fig. 7 shows the density field at different times for $\beta = 1$ and $\Delta R_{CB} = 0.5$. After the initial diffusive transient (Fig. 7(a and b)), due to the existence of a local maximum in the density profile the convective instability begins to grow with fingers of a given wavelength (Fig. 7(c)) that sink towards the bottom gradually (Fig. 7(d–f)). However, the local maximum in the density profile has a relatively small value and this limits the growth of the convective instability. The number of regular fingers formed soon after the onset of the instability is equal to 12, which is equivalent to a wavenumber $k \sim 0.0245$ and a wavelength of ~ 256 . It is to be noted from the linear stability predictions that, for $\Delta R_{cr}'$, the wavenumber for the fingering instability is $k \sim 0.025$.

We now analyze the effect of increasing ΔR_{CB} . Fig. 8 shows the density fields for $\beta = 1$ and $\Delta R_{CB} = 2$ in regime VB ($\Delta R_{CB} > \Delta R'''$) with density profiles such that $\rho_1 > \rho_b$. After the initial diffusive transient, the fingering instability occurs sooner at $t \sim 600$ (Fig. 8(a)). The number of regular fingers formed is 54, which is equivalent to a wavelength ~ 57 and wavenumber $k \sim 0.11$. The intensity of the local maximum in the density profiles is stronger than that for $\Delta R_{CB} = 0.5$. This gives rise to a rapid merging of the fingers that sink towards the bottom (Fig. 8(b–e)). The fingering pattern primarily occurs due to the sinking of the dense product C towards the bottom and by continuity, the displacement of B from the bottom towards the reaction front.¹⁹ This implies the presence of more reactant B at the reaction front to react with A and consequently an increase in the dissolution flux of A . Rapid merging and birth of

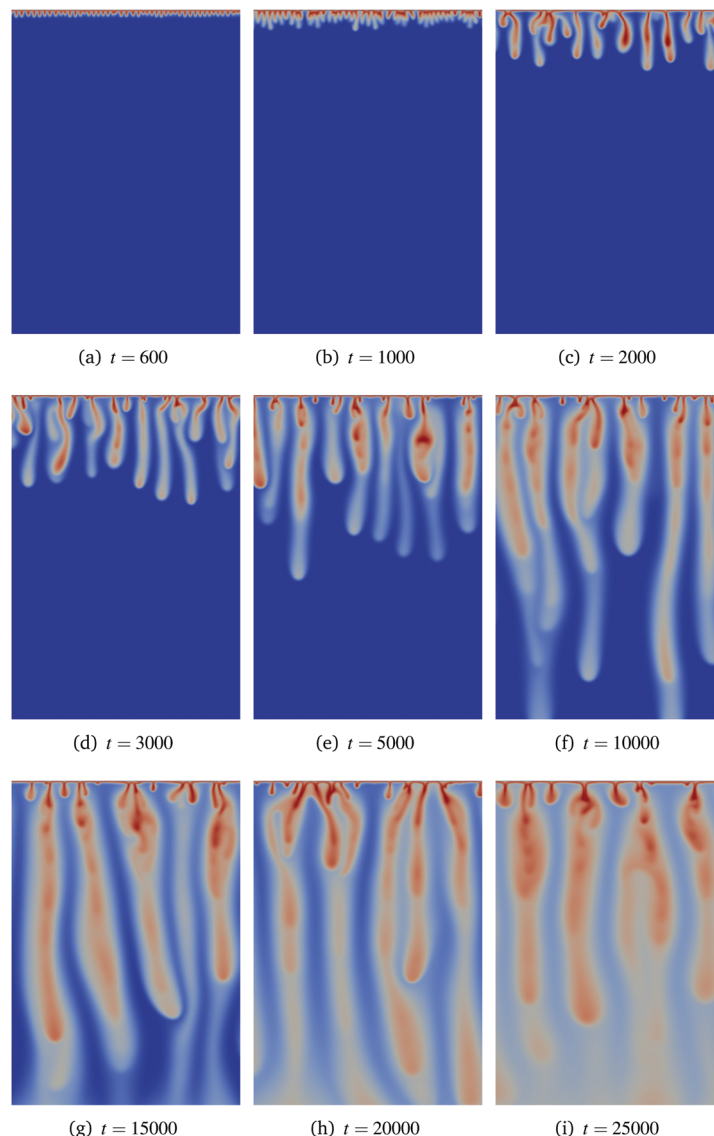


Fig. 8 Regime VB: density field at different times for $\beta = 1$, $\Delta R_{CB} = 2$ and $R_A = -1$ for height $H = 4096$. The scale varies between 0 (blue) and 2 (red).

new fingers that join the old ones, known as protoplumes, is seen to occur. This facilitates enhanced convection and improved mixing. Eventually, the fingers reach the bottom (Fig. 8(f) and (g)) and the system transitions to a shut-down regime. In order to compute the asymptotic properties of the dynamics, we carry out simulations using a larger domain height *i.e.* $H = 4096$. We note that the evolution of the convective dynamics is qualitatively similar to that seen for the non-reactive case⁵ and for the reactive case when the dissolving species *A* increases the density of the host solution and product *C* is denser than reactant *B* ($\Delta R_{CB} > 0$).^{19,24}

We have seen that above the critical value $\Delta R_{cr}'$ for a given β , an increase in ΔR_{CB} fastens the convective dynamics significantly. Next, we analyze the effect of varying β .

5.2 Effect of β on the convective dynamics

The effect of β (and ΔR_{CB}) on the spatio-temporal dynamics can be visualized in Fig. 9 in terms of the spacetime plots of the

density computed at location $z = 128$ below the interface for $\beta = 0.5, 1$ and 1.5 and $\Delta R_{CB} = 0.5$ and 1.5 . This location is chosen such that it is sufficiently below the stable boundary layer to follow the convective dynamics. For $\beta = 0.5$, the lowest value of ΔR_{CB} at which convection occurs is equal to 0.7 and the dominance of diffusion as the transport mechanism is evident here for $\Delta R_{CB} = 0.5$ whereas for $\Delta R_{CB} = 1.5$, the convective instability grows slowly at $t \sim 5000$ in the form of fingers that sink towards the bottom and start merging at $t \sim 10000$. As mentioned in the previous subsection, the critical value for the onset of convection for $\beta = 1$ is $\Delta R_{CB} = 0.35$ that is smaller than the critical value for $\beta = 0.5$. In that case, the convective instability occurs sooner followed by a rapid merging of the fingers for $\Delta R_{CB} = 1.5$. For $\beta = 1.5$, the fingering instability occurs even sooner followed by a rapid merging of the fingers with a lower critical value of $\Delta R_{CB} = 0.25$. This confirms the destabilizing effect of both increasing ΔR_{CB} and β on the

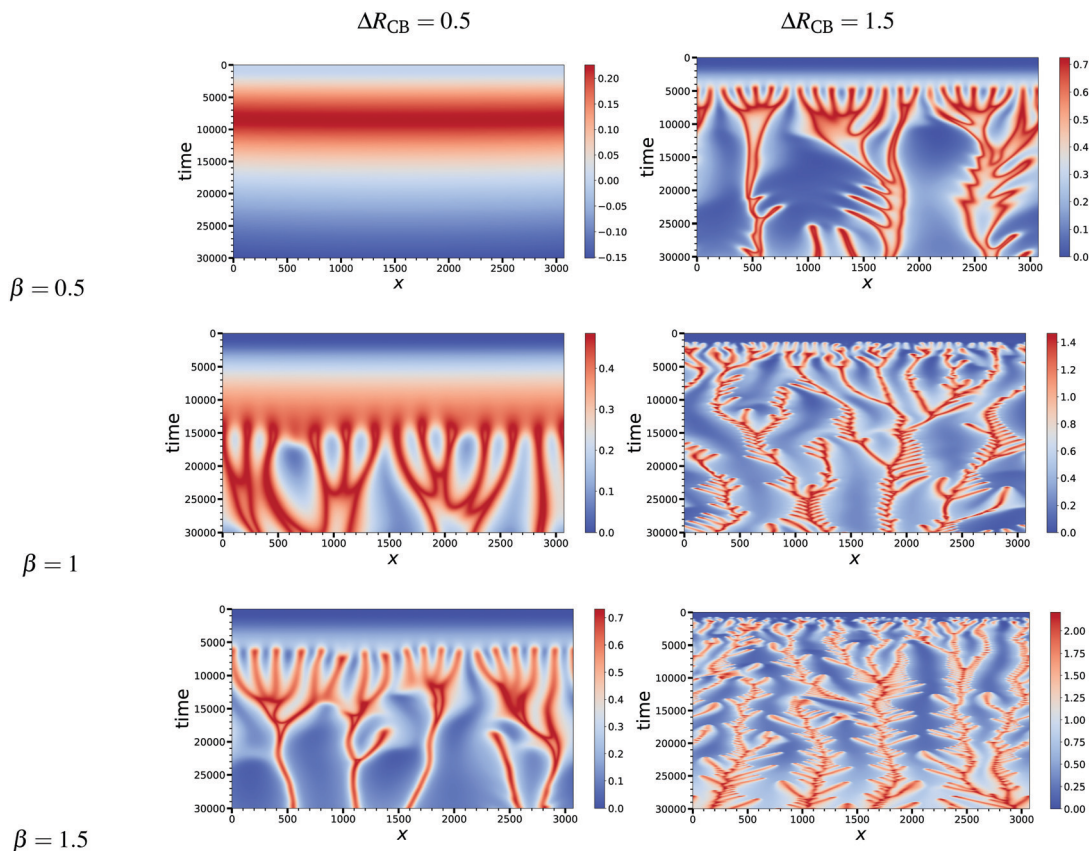


Fig. 9 Spacetime plot of the density computed at $z = 128$ below the interface for different β and left: $\Delta R_{CB} = 0.5$, right: $\Delta R_{CB} = 1.5$. An increase in ΔR_{CB} has a destabilizing effect which results in a decrease of the wavelength of the fingers. This effect is amplified by increasing β .

convective dynamics. For a given β , the critical values above which convection occurs are compared with the predictions made by the linear stability analysis in Fig. 6 to find a good agreement between the two. With an increase in β , the critical value of ΔR_{CB} for the onset of convection drops, shrinking the stable region below, similar to the behaviour observed for ΔR_{cr} and $\Delta R_{cr}'$.

To quantify the storage capacity of species A in the host solution, we compute the dissolution flux J as

$$J = -\frac{1}{L} \int_0^L \frac{\partial A}{\partial z} \Big|_{z=0} dx. \quad (11)$$

The equivalent for the non-reactive case is purely diffusive and given as $J_{NR} = J_D = 1/\sqrt{\pi t}$. The temporal evolution of the dissolution flux J is shown in Fig. 10 for different β and ΔR_{CB} . One curve represents the average over 15 realizations with different initial noise of a given amplitude shown in eqn (5a). The 95% confidence interval shown as lighter areas around the curves represents the variability due to the random noise on the initial condition. Initially, the flux follows the non-reactive one as long as diffusion remains the dominant transport mechanism. After some time, if ΔR_{CB} is above the critical value, the flux deviates from the diffusive one due to the onset of convection and eventually fluctuates around an asymptotic value J^* . For $\beta = 0.5$, shown in Fig. 10(a), the convection begins above $\Delta R_{CB} = 0.7$ and the dissolution flux differs slightly from the

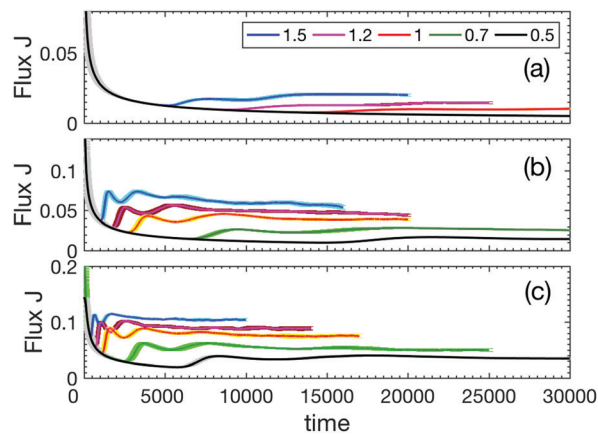


Fig. 10 Temporal evolution of the dissolution flux J for different ΔR_{CB} indicated in the inset and (a) $\beta = 0.5$, (b) $\beta = 1$, (c) $\beta = 1.5$. The critical ΔR_{CB} above which convection occurs for 0.7, 0.35, 0.25, respectively. The 95% confidence interval is shown by the lighter areas around the curves.

diffusive one. Thereafter, with an increase in ΔR_{CB} , the convection sets in at earlier times. For higher values of β , typically, after the initial diffusive transient the flux peaks at two values before reaching a steady regime, which is similar to that seen for the unstable stratifications ($R_A > 0$) with^{19,24} or without reactions.⁵ This trend in the dissolution flux can be seen for $\beta = 1$, shown in Fig. 10(b) for $\Delta R_{CB} = 1, 1.2$ and 1.5 whereas the

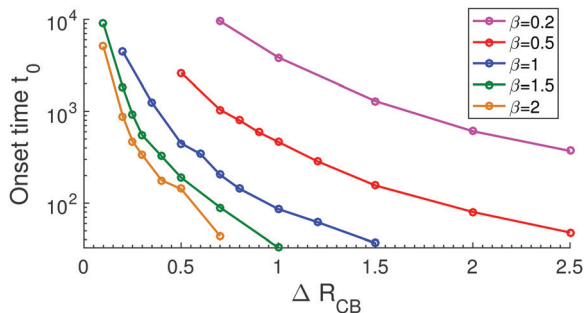


Fig. 11 Onset time for convection t_0 as a function of ΔR_{CB} for the different β indicated in the inset.

second peak in J is rather mild for $\Delta R_{CB} = 0.7$ and J deviates only slightly from the diffusive one for $\Delta R_{CB} = 0.5$. As seen earlier, for $\beta = 1$, the critical value above which convection occurs is $\Delta R_{CB} = 0.35$. Similarly, the peaks in the values of J can be seen for $\beta = 1.5$, shown in Fig. 10(c) for all the values of ΔR_{CB} except for $\Delta R_{CB} = 0.5$, where the second peak is rather mild.

We now analyze the onset time t_0 of the convective instability, defined based on the magnitude of the velocity field computed as $U^2(t) = \int_0^H \int_0^L [u^2(x, z, t) + v^2(x, z, t)] dx dz$. For any value of ΔR_{CB} above the critical $\Delta R_{cr}'$, U^2 first decreases until a given onset time t_0 when it reaches its minimum before it begins to grow^{5,19} due to the onset of the convective instability. The onset time t_0 for this instability is shown in Fig. 11 for various values of ΔR_{CB} and β . An increase in ΔR_{CB} for a given β leads to a decrease in the values of t_0 by orders of magnitude and this effect is even stronger with larger β .

Next, we quantify in Fig. 12 the asymptotic dissolution flux J^* for all the cases studied here with $R_A = -1$. As $\beta \rightarrow 0$ and $\Delta R_{CB} \rightarrow 0$, the dynamics are similar to the non-reactive one, where diffusion is the dominant transport mechanism. We only plot here the asymptotic dissolution flux for the cases where convection occurs. The asymptotic dissolution flux J^* increases

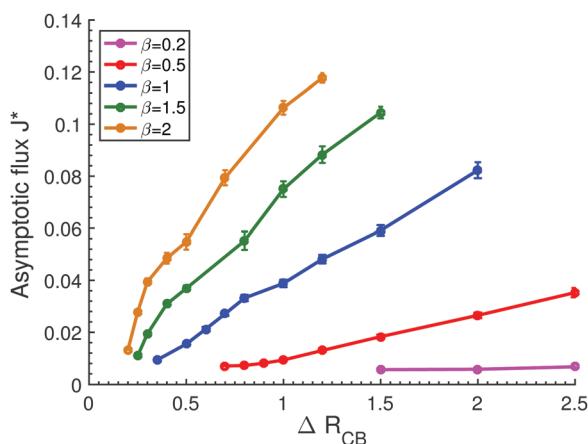


Fig. 12 Asymptotic dissolution flux J^* as a function of ΔR_{CB} above the critical value for different β indicated in the inset for $R_A = -1$. The corresponding non-reactive case is purely diffusive and is given by $J_{NR} = 1/\sqrt{\pi t}$.

with an increase in β and ΔR_{CB} . This increase in J^* can be explained as follows. When the contribution to density of the product C is significantly larger than that of the reactant B , convection occurs at earlier times and the dense fingers formed reach the bottom rapidly, causing a depletion of B at the reaction front and due to continuity, more reactant B is then transported from the bottom to the reaction front to react with A . The strong convective motions leads to improved mixing and a consequently faster dissolution flux of A into the host solution. This motion can be further enhanced and the asymptotic dissolution flux can be increased by an order of magnitude by increasing β .

To summarize this section, we have shown by nonlinear simulations that in a stable density stratification where dissolution is entirely controlled by diffusion in the non-reactive case, $A + B \rightarrow C$ reactions can trigger convection. Specifically, increasing the difference ΔR_{CB} in the contribution to density between the product C and reactant B above a critical value, it is possible to initiate the convective instability and achieve enhanced asymptotic dissolution fluxes. For a given β , the critical values of ΔR_{CB} above which convection develops in the nonlinear simulations are in good agreement with those predicted by the linear stability analysis, $\Delta R_{cr}'$. This critical value for the onset of convection can be reduced by increasing β . Thus, both β and ΔR_{CB} have a destabilizing effect on the convective dynamics of the process.

6 Conclusions

We have numerically studied the reaction-driven convective dynamics developing when a species A dissolves into a host solution containing a solute B to produce C via an $A + B \rightarrow C$ type of reaction and all the species diffuse at equal rates. We have focussed here on the case where the dissolving species decreases the density of the host phase upon dissolution ($R_A < 0$) and the density stratification is stable in the absence of reactions. While it is known that reactions induce convection in such stable stratifications¹⁹ when C is denser than B , we have obtained here the critical conditions for the onset of convection as a function of the difference $\Delta R_{CB} = R_C - R_B$ in the contribution to density between the product C and the reactant B and the ratio $\beta = B_0/A_0$ of the initial concentrations of the reactant B and the solubility of A using linear stability analysis and nonlinear simulations. We have further analyzed the convective dynamics and dissolution fluxes for different values of ΔR_{CB} and β to show that chemical reactions can increase storage rates with regard to the non-reactive case.

The monotonically decreasing density profiles for the non-reactive equivalent can be modified, with the help of reactions, to exhibit a local maximum when C is denser than B . These non-monotonic profiles of the stable regime IVB transition to the unstable regime V above a critical value of $\Delta R_{CB} = R_C - R_B$ for a given β . The unstable non-monotonic density profiles can be classified based on the amplitude of the end point values ρ_1 and ρ_b such that in regime VA the density at the interface ρ_1 is smaller than or equal to the initial density ρ_b of the host phase

whereas, in regime VB, we have $\rho_I > \rho_b$. However, for all the values of parameters studied here, the critical condition for the onset of convection occurs when $\rho_I < \rho_b$ i.e. in regime VA.

First, we studied the linear stability of the non-monotonic density profiles using a frozen time or quasi-steady-state approximation to identify the critical conditions for the convective instability. We computed the neutral stability boundary, denoted by ΔR_{cr} , above which the growth rate is positive and the system is linearly unstable to infinitesimal perturbations. However, slightly above this critical value, the growth rate of the least stable eigenmode is too small, of the order 10^{-4} , and a large time is needed for this instability to develop. Therefore, we also computed a characteristic growth rate, defined as the maximum growth rate at a frozen time t_f for which the amplification factor of the perturbation is of order unity. More precisely, the critical condition for which $\sigma_{max} * t_f = 1$ is referred to as $\Delta R_{cr}'$. Above this critical value, a sufficiently dense layer of fluid is formed locally overlying the host solution such that it is able to trigger the convective instability. We found that both ΔR_{cr} and $\Delta R_{cr}'$ decrease with an increase in β . Thus, the linear stability results suggest that increasing ΔR_{CB} or β has a destabilizing effect.

Next, we performed nonlinear simulations to identify the critical values of ΔR_{CB} above which convection occurs for the different β studied here and found a good agreement with the predictions made by the linear stability analysis for $\Delta R_{cr}'$. This suggests that the onset of convection in nonlinear simulations is better captured by searching for a criterion such as $\sigma_{max} * t_f = 1$ in the LSA rather than simply $\sigma = 0$. Similar conclusions have been discussed in an experimental analysis of the onset of convection driven by the dissolution of CO_2 in water and salt solutions.⁸

When the difference between the contribution to density of the product C and reactant B is increased above the critical value $\Delta R_{cr}'$, the local maximum in the density stratification becomes stronger and gives rise to an earlier onset of the fingering instability and rapid mixing. The critical value of ΔR_{CB} above which convection occurs drops with an increase in β and for a larger β the destabilizing effect of increasing ΔR_{CB} is even stronger. Thus, upon increasing ΔR_{CB} and β , it is possible to amplify the intensity of the local maximum in the density profiles, which in turn leads to enhanced convection. This destabilizing effect can be seen in the temporal evolution of the dissolution flux of species A , where the departure from a diffusive regime occurs sooner with increased asymptotic dissolution flux J^* for increasing β and ΔR_{CB} . An order of magnitude increase in the asymptotic dissolution flux can be achieved. Similarly, the onset time t_0 for convection reduces by orders of magnitude when β and ΔR_{CB} are increased. Conversely, when $\beta \rightarrow 0$, the non-reactive case is recovered where diffusion is the dominant transport mechanism.

Our results show that chemical reactions have a strong potential to initiate convection beyond a certain critical value of ΔR_{CB} and impact the convective dissolution process significantly leading to improved mixing in various geological situations that involve initially stable density stratifications. In the

context of CO_2 sequestration, such stratifications occur either when there exist pockets of dense CO_2 -rich brine underneath the less dense brine or when CO_2 is pumped at the bottom of aquifers as opposed to at the top. Reactions can then enhance the dissolution fluxes and increase the storage rates by an order of magnitude. Thus, the chemical composition of the geological storage site is an important factor in determining the success of the sequestration technique. The results presented here open an avenue for experimentalists to verify our theoretical predictions.

Conflicts of interest

There are no conflicts to declare.

Acknowledgements

We thank B. Knaepen and V. Loodts for their help and support concerning the YALES2 code. We gratefully acknowledge the financial support from the Fondation ULB and from the FRS-FNRS PDR CONTROL project.

Notes and references

- 1 Intergovernmental Panel on Climate Change (IPCC) special report on Carbon Dioxide Capture and Storage, Cambridge University Press, New York, 2005.
- 2 G. S. Pau, J. B. Bell, K. Pruess, A. S. Almgren, M. J. Lijewski and K. Zhang, *Adv. Water Resour.*, 2010, **33**, 443–455.
- 3 M. T. Elenius and K. Johannsen, *Comput. Geosci.*, 2012, **16**, 901–911.
- 4 A. C. Slim, M. M. Bandi, J. C. Miller and L. Mahadevan, *Phys. Fluids*, 2013, **25**, 024101.
- 5 A. C. Slim, *J. Fluid Mech.*, 2014, **741**, 461–491.
- 6 H. E. Huppert and J. A. Neufeld, *Annu. Rev. Fluid Mech.*, 2014, **46**, 255–272.
- 7 H. Emami-Meybodi, H. Hassanzadeh, C. P. Green and J. Ennis-King, *Int. J. Greenhouse Gas Control*, 2015, **40**, 238–266.
- 8 C. Thomas, S. Dehaeck and A. De Wit, *Int. J. Greenhouse Gas Control*, 2018, **72**, 105–116.
- 9 J. Ennis-King and L. Paterson, *Int. J. Greenhouse Gas Control*, 2007, **1**, 86–93.
- 10 C. Wylock, A. Rednikov, B. Haut and P. Colinet, *J. Phys. Chem. B*, 2014, **118**, 11323–11329.
- 11 M. A. Budroni, L. A. Riolfo, L. Lemaigre, F. Rossi, M. Rustici and A. De Wit, *J. Phys. Chem. Lett.*, 2014, **5**, 875–881.
- 12 V. Loodts, C. Thomas, L. Rongy and A. De Wit, *Phys. Rev. Lett.*, 2014, **113**, 114501.
- 13 S. S. S. Cardoso and J. T. H. Andres, *Nat. Commun.*, 2014, **5**, 5743.
- 14 V. Loodts, L. Rongy and A. De Wit, *Phys. Chem. Chem. Phys.*, 2015, **17**, 29814.
- 15 V. Loodts, P. M. J. Trevelyan, L. Rongy and A. De Wit, *Phys. Rev. E*, 2016, **94**, 043115.

- 16 C. Thomas, V. Loodts, L. Rongy and A. De Wit, *Int. J. Greenhouse Gas Control*, 2016, **53**, 230–242.
- 17 I. Cherezov and S. S. S. Cardoso, *Phys. Chem. Chem. Phys.*, 2016, **18**, 23727–23736.
- 18 C. Wylock, A. Rednikov, P. Colinet and B. Haut, *Chem. Eng. Sci.*, 2017, **157**, 232–246.
- 19 V. Loodts, B. Knaepen, L. Rongy and A. De Wit, *Phys. Chem. Chem. Phys.*, 2017, **19**, 18565–18579.
- 20 P. Ghoshal, M. C. Kim and S. S. S. Cardoso, *Phys. Chem. Chem. Phys.*, 2017, **19**, 644–655.
- 21 M. A. Budroni, C. Thomas and A. De Wit, *Phys. Chem. Chem. Phys.*, 2017, **19**, 7936.
- 22 V. Loodts, H. Saghrou, B. Knaepen, L. Rongy and A. De Wit, *Fluids*, 2018, **3**, 83.
- 23 M. C. Kim and S. S. S. Cardoso, *Phys. Fluids*, 2018, **30**, 094102.
- 24 M. Jotkar, A. De Wit and L. Rongy, *Phys. Chem. Chem. Phys.*, 2019, **21**, 6432–6442.
- 25 O. Citri, M. L. Kagan, R. Kosloff and D. Avnir, *Langmuir*, 1990, **6**(3), 0743–7463.
- 26 A. J. Pons, F. Sagués, M. A. Bees and P. G. Sorensen, *J. Phys. Chem. B*, 2000, **104**, 2251–2259.
- 27 M. A. Bees, A. J. Pons, P. G. Sorensen and F. Sagués, *J. Chem. Phys.*, 2001, **114**, 1932.
- 28 A. J. Pons, F. Sagués, M. A. Bees and P. G. Sorensen, *J. Phys. Chem. B*, 2002, **106**, 7252–7259.
- 29 A. J. Pons, O. Batiste and M. A. Bees, *Phys. Rev. E*, 2008, **78**, 016316.
- 30 M. Bestehorn and A. Firoozabadi, *Phys. Fluids*, 2012, **24**, 114102.
- 31 N. Tilton, D. Daniel and A. Riaz, *Phys. Fluids*, 2013, **25**, 092107.
- 32 V. Moureau, P. Domingo, L. Vervisch and A. Riaz, *C. R. Mech.*, 2011, **339**, 141–148.
- 33 V. Loodts, PhD thesis, Université libre de Bruxelles, 2016.
- 34 D. A. Rees, A. Selim and J. P. Ennis-King, *Emerging Topics in Heat and Mass Transfer in Porous Media Theory and Application of Transport in Porous Media*, 2008, vol. 22, pp. 85–110.
- 35 M. C. Kim and C. K. Choi, *Phys. Fluids*, 2012, **24**, 044102.
- 36 C. Canuto, M. Y. Hussaini, A. Quarteroni and T. A. Zang, *Spectral Methods. Fundamentals in Single Domains*, Springer, 2006.
- 37 Y. Saad, *Numerical methods for large eigenvalue problems*, Manchester University Press, 1992.
- 38 P. M. J. Trevelyan, C. Almarcha and A. De Wit, *J. Fluid Mech.*, 2011, **670**, 38–65.